An Algorithm for Merging SMAP Radiometer and Radar Data for High Resolution Soil Moisture Retrieval

Narendra N. Das
Dara Entekhabi
Eni G. Njoku

Manuscript received on Dec 21, 2009; revised on Apr 27, 2010 and Sep 03, 2010.

N. N. Das is with Jet Propulsion Laboratory, California Institute of Technology, Pasadena, Ca 91109 USA (email: nndas@jpl.nasa.gov). Corresponding author.

D. Entekhabi is with Department of Civil and Environmental Engineering, Massachusetts Institute of Technology, Cambridge, MA 02139 USA (email: darae@mit.edu).

E. G. Njoku is with Jet Propulsion Laboratory, California Institute of Technology, Pasadena, Ca 91109 USA (email: eni.g.njoku@jpl.nasa.gov).

Digital Object Identifier TGRS-2009-00901.R2

This work was carried out in part at the Jet Propulsion Laboratory, California Institute of Technology, under contract with the National Aeronautics and Space Administration.

Abstract

A robust and simple algorithm is developed to merge L-band radiometer retrievals and L-band radar observations to obtain high-resolution (9 km) soil moisture estimates from data of the NASA Soil Moisture Active and Passive (SMAP) mission. The algorithm exploits the established accuracy of coarse-scale radiometer soil moisture retrievals and blends this with the fine-scale spatial heterogeneity detectable by radar observations to produce a high-resolution optimal soil moisture estimate at 9 km. The capability of the algorithm is demonstrated by implementing the approach using the airborne Passive and Active L-band System (PALS) instrument dataset from Soil Moisture Experiments, 2002 (SMEX02) and a four-month synthetic data set in an Observation System Simulation Experiment (OSSE) framework. The results indicate that the algorithm has potential to obtain better soil moisture accuracy at a high resolution, and show an improvement in root-mean-square-error of 0.015 to 0.02 cm^3/cm^3 volumetric soil moisture over the minimum performance taken to be retrievals based on radiometer measurements re-sampled to a finer scale. These results are based on PALS data from SMEX02 and four-months of OSSE dataset, and need to be further confirmed for different hydroclimatic regions using airborne dataset from prelaunch calibration/validation field campaigns of the SMAP mission.

Index Terms

SMAP, L-band, radiometer, radar, soil moisture

1. Introduction

Soil moisture is a land state variable that controls several water cycle fluxes, namely runoff, evapotranspiration, and deep drainage. In addition, soil moisture modulates the energy cycle through exchanges of energy between the atmosphere and the land surface. Soil moisture and its freeze/thaw state are also key determinants of the carbon exchange at the land surface. Thus, global measurements of soil moisture are vital to understanding the components and interactions between the global water, energy and carbon cycles. Satellite-based microwave remote sensing is the most promising technique for providing global measurements of near-surface soil moisture, with frequent revisit, and independent of clouds and solar illumination. Many satellite-based microwave instruments, e.g., the Scanning Multichannel Microwave Radiometer (SMMR), Special Sensor Microwave Imager (SSM-I), and Advanced Microwave Scanning Radiometer (AMSR-E) have demonstrated this capability. However, these sensors operate at C-band (~6 GHz) and higher frequencies, and their soil moisture retrievals are significantly affected by even small amounts of vegetation cover. The recently launched Soil Moisture and Ocean Salinity (SMOS) mission of the European Space Agency will be the first wide-swath L-band soil moisture mission, and has the potential for retrieving soil moisture over a much higher range of vegetation conditions. The measurements from these radiometer instruments have coarse spatial resolution >40 km, which is sufficient for hydroclimate applications. However, for hydrometeorological applications soil moisture measurements of ~10 km spatial resolution [1] or better are required with a temporal resolution of 3 days or less. The ~10 km resolution requirement is also derived from several applications in hydrologic and atmospheric science, which have

distinguishing features or significant physical interactions at the hydrometeorological (~10 km) scale. The spatial resolution of ~10 km is estimated as a multiple of the blending height in the atmosphere. Hydrometeorological events such as precipitating systems and thermal convection are affected by near-surface atmospheric variations. For example, there is evidence that irrigation in Nebraska has changed the amount of precipitation in Iowa, and irrigation in Texas has led to an increase in tornado activity [2]. Availability of a ~10 km soil moisture product would enhance understanding and forecast capabilities of regional weather systems around the world. Furthermore, it is anticipated that within the 2010-2015 time frame global numerical weather prediction (NWP) models will be implemented on a 10 km grid scale. Soil moisture is a prognostic and a boundary condition in these NWP models. The accuracy/skill of the forecasts for a given NWP model depends largely on model initialization and boundary conditions. Numerous data-denial experiments have demonstrated the influence of accurate soil moisture initialization and boundary condition on the forecast skill of variables such as precipitation, air temperature, air humidity, cloudiness, etc. NWP Centers currently use climatology or soil moisture accounting model estimates (forced with surface precipitation, surface incident radiation, etc.). The availability of fine scale (~10 km) soil moisture data will also benefit agriculture-related applications and large watershed or river-basin management activities. Realizing the importance of fine resolution, global soil moisture measurements, the National Research Council's Committee on Earth Science and Applications from Space recommended the Soil Moisture Active and Passive (SMAP) mission, with the objective to produce soil moisture data products for hydrometeorological applications, as one of four recommended first-tier missions [3]. In

2008 NASA selected SMAP for development [4]. The mission is targeted for launch in 2014.

The SMAP instrument architecture incorporates an L-band radar (frequency: 1.26 GHz; polarizations: HH, VV, HV) and an L-band radiometer (frequency: 1.41 GHz; polarizations: H, V, U) that share a single feedhorn and parabolic mesh reflector. The reflector (diameter: 6 m) is offset from nadir and rotates about the nadir axis at 14.6 rpm, providing a conically-scanning antenna beam with a constant surface incidence angle of approximately 40°. SMAP will be launched into a 680 km near-polar, sun-synchronous orbit with an 8-day repeat cycle and Equator crossings at 6 am and 6 pm local time. At this altitude, the antenna scan configuration yields a 1000-km swath, with a 40 km radiometer resolution and 1-3 km synthetic aperture radar (SAR) resolution (over the outer 70% of the swath) that provides global coverage within 3 days at the Equator and 2 days at boreal latitudes (>45°N). The primary requirement of SMAP is to provide estimates of soil moisture in the top 5 cm of soil with an accuracy of 0.04 cm^3/cm^3 volumetric soil moisture, at 10 km resolution, with 3-day average intervals over the global land area excluding regions of snow and ice, mountainous topography, open water, and vegetation with total water content greater than 5 kg/m^2.

The expected suite of products from the SMAP mission is shown in Table 1. In this paper we address primarily the soil moisture products. The Level 2 radiometer-only soil moisture product (L2_SM_P) is derived principally from the brightness temperature product (L1C_TB). L-band radiometer algorithms for soil moisture retrieval are well established, with less error and better quantification of uncertainties under vegetated conditions than radar algorithms [5]; however radiometers suffer from coarse spatial

resolution (~40 km for SMAP). The radar-only soil moisture (L2_SM_A) is a fine-resolution (3 km) soil moisture product derived from the Hi-Res radar backscatter data (L1C_S0_HiRes). Studies (e.g., [6]) have shown that soil moisture measurements derived from radar backscatter have uncertainty/errors that are sensitive to even sparse vegetation cover. This makes radar soil moisture retrievals less useful in vegetated areas for applications with high accuracy requirements. Radar backscatter is highly influenced by surface roughness, canopy structure, and vegetation water content (VWC) in addition to soil moisture. Roughness and vegetation effects significantly reduce the sensitivity of radar backscatter to soil moisture.

For the above reasons, neither the SMAP radiometer nor the radar can individually meet the SMAP requirements for soil moisture spatial resolution (10 km) and accuracy (0.04 cm^3/cm^3). We propose here an algorithm that overcomes these limitations by merging the active (radar) and passive (radiometer) measurements to derive a 9 km soil moisture product (L2_SM_A/P) that meets the SMAP requirements. The algorithm is based on the radar capability to detect high-resolution soil moisture spatial variability within the coarse-resolution radiometer L2_SM_P grid. The algorithm approximates as near-linear the relationship between L-band radar backscatter and volumetric soil moisture for both bare and vegetated surfaces. The relationship is described by a regression slope that is determined from time series radar co-polarized backscatter (L1C_S0_HiRes) and volumetric soil moisture (L2_SM_P) data. The feasibility of using time series data to compute the regression slope has been demonstrated in [7]-[9]. To estimate the soil moisture for L2_SM_A/P, the relative backscatter difference within the coarse grid of L2_SM_P is then constrained with the

regression slope and the higher-accuracy L2_SM_P soil moisture. The following section elaborates the mathematical formulation of the algorithm, and discusses the novelty of this approach with respect to other time series algorithms [8], [9].

2. Active/Passive Retrieval Algorithm

For clarity, we first define general grid topologies, mathematical operators, and terms used in the mathematical formulation. Figure 1 elaborates the nested grid topology of the L2_SM_P (36 km), L1C_S0_HiRes (3 km), and desired merged Active/Passive L2_SM_A/P (9 km) products. For convenience in mathematical formulation, the naming convention of '*C*' (coarse), '*F*' (fine), and '*M*' (medium) for the L2_SM_P, L1C_S0_HiRes, and L2_SM_A/P grid scales, respectively, is used throughout this section. It is seen from the grid topology (Fig. 1) that within a single (nc = 1) 36 km x 36 km pixel of grid *C* there are n = 16 pixels of grid *M*, nf = 144 pixels of grid *F*, and m = 9 i.e, number of F grid cells within M.

Two linear operators used frequently in the mathematical formulation are defined as:

Spatial average operator: $\langle x \rangle = \frac{1}{A} \int x \, da$

Spatial anomaly operator: $\delta x = x - \langle x \rangle$

Here, A is the area of a larger pixel and a is the area of a smaller pixel within A;

Relationships between co-polarized radar backscatter at L-band and C-band and volumetric soil moisture have been discussed in [5]-[7]. At L-band, a near-linear relationship was found using truck-mounted radar data collected during the Washita 92 field experiment [7]. A linear relationship between radar backscatter at L-band and

volumetric soil moisture was also reported for airborne observations in the Soil Moisture Experiment, 2002 (SMEX02) [8]. The formulation of the algorithm discussed here is based on such a linear relationship. We use the hypothesis that the volumetric soil moisture and co-polarized backscatter are linearly related through:

$$\theta(t) = \alpha + \beta \log[\sigma(t)] \quad (1)$$

At a given scale, α and β are parameters that depend on vegetation cover and type as well as surface roughness. They vary seasonally and can be estimated at scale C using SMAP L2_SM_P and L1C_S0_HiRes data time-series as regressant and regressors as in

$$\theta(C,t) = \alpha(C) + \beta(C)\langle \log[\sigma(M_n,t)] \rangle \quad (2)$$

Here, $\sigma(M_n,t)$ is co-polarized radar backscatter at spatial scale M, and $\theta(C,t)$ is volumetric soil moisture at spatial scale C. In this section *log* represents $10log_{10}$. The co-polarized backscatter $\sigma(M_n,t)$ is obtained by aggregating $\sigma(F_m,t)$ within M, which is effective for reducing speckle noise. The estimation of parameters $\alpha(C)$ and $\beta(C)$ uses a time sequence of SMAP data, implying that this is a time-series approach. The algorithm takes advantage of the conical scan and constant look-angle of the antenna beam approach of SMAP. Except where azimuthal effects are significant, the constant look-angle reduces the variations in the $\alpha(C)$ and $\beta(C)$ parameters.

Formulation of the algorithm begins with the hypothesized linear relationship between volumetric soil moisture and co-polarized radar backscatter at spatial scale M, so that (1) can be written as

$$\theta(M_n,t) = \alpha(M_n) + \beta(M_n) \log[\sigma(M_n,t)] \quad (3)$$

where $\alpha(M_n)$ and $\beta(M_n)$ are empirical parameters at spatial scale of M, and $\theta(M_n,t)$ is a soil moisture value at a spatial scale of M and at time t for a particular pixel within C. By spatially averaging both side of (3), we obtain:

$$\begin{aligned}\langle\theta(M_n,t)\rangle &= \langle\alpha(M_n)+\beta(M_n)\log[\sigma(M_n,t)]\rangle \\ &= \langle\alpha(M_n)\rangle+\langle\beta(M_n)\log[\sigma(M_n,t)]\rangle\end{aligned} \tag{4}$$

Subtracting (4) from (3) gives

$$\begin{aligned}\delta\theta(M_n,t) &= \theta(M_n,t)-\langle\theta(M_n,t)\rangle \\ &= \alpha(M_n)+\beta(M_n)\log[\sigma(M_n,t)]-\langle\alpha(M_n)\rangle-\langle\beta(M_n)\log[\sigma(M_n,t)]\rangle \\ &= \{\alpha(M_n)-\langle\alpha(M_n)\rangle\}+\{\beta(M_n)\log[\sigma(M_n,t)]-\langle\beta(M_n)\log[\sigma(M_n,t)]\rangle\}\end{aligned} \tag{5}$$

A major assumption is now introduced that allows development of a robust algorithm, but at the cost of increased error due to land cover heterogeneity. It is assumed that significant variations in the parameters $\alpha(M_n)$ and $\beta(M_n)$ related to vegetation type, vegetation cover and surface roughness are homogeneous within C. In this case $\alpha(M_n)=\langle\alpha(M_n)\rangle=\alpha(C)$ and $\beta(M_n)=\langle\beta(M_n)\rangle=\beta(C)$. Now (5) becomes:

$$\delta\theta(M_n,t)=\beta(C)\{\log[\sigma(M_n,t)]-\langle\log[\sigma(M_n,t)]\rangle\} \tag{6}$$

The complete algorithm for the hydrometeorological scale (9 km) soil moisture $\theta(M_n,t)$ can then be written using (5), (6), and $\langle\theta(M_n,t)\rangle = \theta(C,t)$, as

$$\begin{aligned}\theta(M_n,t) &= \theta(C,t)+\delta\theta(M_n,t) \\ &= \theta(C,t)+\beta(C)\{\log[\sigma(M_n,t)]-\langle\log[\sigma(M_n,t)]\rangle\}\end{aligned} \tag{7}$$

The parameter $\beta(C)$ is based on the time-series regression in (2). This is similar to the determination of time-series regression parameters discussed in [8]. $\theta(C,t)$ in (2) and (7) are obtained from the SMAP L2_SM_P product, $\log[\sigma(M_n,t)]$ and its spatial average $\langle\log[\sigma(M_n,t)]\rangle$ are obtained from the SMAP L1C_S0_HiRes product, and then linear regression is performed to obtain $\beta(C)$. The main assumption of the algorithm concerning

the scales of heterogeneity of parameter β can be relaxed as the repeated application of the algorithm shows a consistent relationship between β and vegetation/surface characteristics. Results from *Du et al.* [10] indicate that the relative sensitivity of L-band co-polarized radar channels depends primarily on the vegetation canopy opacity (i.e., vegetation water content). Simulations conducted by [9] for L-band co-polarized radar backscatter using the integral equation model show that surface roughness variability has a lesser effect on the radar soil moisture sensitivity. Airborne field experiment data and theoretical models can be used to derive the dependence of co-polarized radar backscatter on vegetation. With such a relationship, high-resolution ancillary data on vegetation (e.g., an optical/infrared vegetation index or *VI*) or a radar vegetation index (*RVI*) [7] derived from SMAP co- and cross-polarized radar data, can be used to adjust the slope parameter β at scale M as in:

$$\beta(M_n, t) = f[\beta(C), VI] \tag{8}$$

Preliminary experiments with numerical simulations and field data indicate that it is indeed possible to formulate such a relationship that will reduce errors of the algorithm. In this study we use the original version of the algorithm given in (7) in order to estimate and understand the upper bound of error in the algorithm.

3. Test Datasets

There are few real and synthetic data sets available to test the algorithm developed here specifically for SMAP mission. Prominent among the available data are the Passive and Active L-band System (PALS) [11] data set from the SGP99, SMEX02, CLASIC and SMAPVEX08 field experiments, and the Hydros Observation System

Simulation Experiment (OSSE) data set [12], [13]. The PALS sensor is an airborne instrument and has a spatial resolution of approximately 0.4 km (depending on flight altitude). The PALS dataset from SMEX02 is used initially to test the algorithm. The reason of using the PALS SMEX02 dataset is the availability wet and dry soil moisture status, and range of vegetation conditions within the PALS flight domain for the campaign duration. PALS was flown over the SMEX02 region (the Walnut Creek watershed, Iowa) for eight days during the months of June and July, 2002. However, to fully test the algorithm performance a synthetic dataset covering a longer time series and a larger regional extent is required. Therefore, the four-month (April 1st, 1994 to July 31st, 1994) OSSE data set created for the Hydros mission was also utilized for algorithm testing. The OSSE data were created by simulating high-resolution land surface geophysical variables from a distributed land surface model (TOPLATS) within the Red-Arkansas river basin. The basin domain and simulation period incorporate a diverse range of land cover classes and soil moisture values. The geophysical variables were used to derive simulated brightness temperatures and radar backscatter cross-sections over the basin according to the Hydros sensor observational configuration (the same configuration used by SMAP). The simulated sensor measurements, with appropriate instrument and environmental noise added, were then inverted to retrieve soil moisture using various retrieval algorithms. The forward models used to derive brightness temperatures and radar backscatter cross-sections are described in detail in [12] and [13]. A caveat of using the forward model as mentioned in [12] and [13] to compute radar backscatter cross-sections is that it does not include the influence of vegetation structure pertaining to different crop types.

The OSSE generated geophysical variables and simulated sensor observations at a spatial resolution of 1 km. Subsequently, the brightness temperatures and radar backscatter cross-sections were aggregated with appropriate errors to simulate the SMAP observations at the radiometer (36 km) and radar (3 km) resolutions. The radiometer-only soil moisture product (L2_SM_P) is derived from the aggregated 36-km brightness temperature [12]. The accuracy of the retrieved L2_SM_P soil moisture product varies with vegetation water content (VWC). For this study we assigned a Root-Mean-Square-Error (RMSE) to the 36-km soil moisture values of 0.01 to 0.04 cm^3/cm^3, linearly with increasing VWC from 0 to 5 kg/m^2, based on the results of [12]. The radar backscatter cross-sections were aggregated to 3 km and a measurement error of K_p = 0.16 was added to simulate the SMAP 3-km radar L1C_S0_HiRes measurements. These data were then spatially aggregated from 3 km to 9 km for input to the algorithm. K_p is the radar normalized measurement relative error that depends on the signal-to-noise ratio (SNR) and the number of independent samples or 'looks' averaged in each measurement. Additional synthetic experiments were conducted by adding K_p error values of 0.18, 0.2, and 0.22 to evaluate the sensitivity of the output soil moisture product (9 km) to K_p errors in $\sigma(M_n,t)$. The results and performance of the algorithm based on these inputs are discussed in the next section.

4. Retrieval Results

4.1. Test of Algorithm using SMEX02 PALS data

This study applies the PALS SMEX02 dataset to the Active/Passive algorithm (Section 2). PALS L-band radar and radiometer have similar frequencies and incidence

angle like SMAP, however, PALS have much finer spatial resolution (~0.8 km). To apply the Active/Passive algorithm, the PALS data were gridded at different resolutions, for radiometer at ~4 km and radar at ~0.8 km. The combination of T_{B_V} and σ_{vv} data from PALS data was considered for Active/Passive algorithm because of higher degree of correlation observed between them. Figure 2 illustrates degree of correlation between T_{B_p} and σ_{pp} for different possible combinations of radar and radiometer data obtained from the PALS data of SGP99, SMEX02, CLASIC and SMAPVEX08, which clearly indicates a better result for T_{B_V} and σ_{vv}. Therefore soil moisture retrieved from T_{B_V} is expected to correlated better with σ_{vv}.

Soil moisture (θ at 4 km) is retrieved from T_{B_V} at 4 km resolution using a microwave emission (Tau-omega) model that is based on a layered single scattering model commonly used for passive microwave sensing at L-band [5]. Ancillary data (e.g., surface soil temperature, soil roughness, vegetation water content) of SMEX02 were used to run the microwave emission model. Figure 3 shows the gridded T_{B_V} (4 km) and corresponding retrieved θ(4 km) as shown in Fig. 3a and 3c. The values of β are estimated using regression on pairs of $\theta(4\ \mathrm{km})$ and $\langle\sigma_{pp}(0.8\ \mathrm{km})\rangle$ for every 4 km grid cells over the SMEX02 duration. The regression yields an error of estimation as well as the expected statistical slope β. The robustness of β is subjected to the number of available $\theta(4\ \mathrm{km})$ and $\langle\sigma_{pp}(0.8\ \mathrm{km})\rangle$ data pairs. For SMEX02 dataset there are 8 such pairs that lead to slightly larger error of estimation for β. However, the derived β was used in the Active/Passive soil moisture disaggregation algorithm (7) for all the sixteen 4 km grid cells within the PALS domain, to disaggregate θ (4 km) to obtain high resolution θ at 0.8 km (Fig. 3d).

To validate the retrieved soil moisture estimates at 0.8 km resolution, the field averaged soil moisture calculated from *in situ* measurements in 31 fields over 4 days (5th July, 2002 to 8th July, 2002) are used (Fig. 4). The representative spatial resolution of a field is nearly ~0.8 km making the comparison compatible. It is obvious from Fig. 4 that even with slightly higher error of estimation for β the Active/Passive algorithm (RMSE: 0.035 [cm^3/cm^3]) outperforms the minimum performance (RMSE: 0.048 [cm^3/cm^3]). The minimum performance is a reference for comparison. It is essentially a resampling of soil moisture at θ (4 km) to finer scale (0.8 km) without use of information from the radar. With decrease in error of estimation for β or in other words increasing the number of data pairs ($\theta(4\text{ km})$ and $\langle\sigma_{pp}(0.8\text{ km})\rangle$) will enhance the robustness of β and consequently decrease the RMSE in the disaggregated high resolution soil moisture estimates. Results from this study establish the applicability of Active/Passive algorithm. However, this study does not address the impact of different levels of noise in radar data on the Active/Passive algorithm because the PALS radar data have a very low noise floor level (~-40 [dB]). The subsequent subsection that utilizes the synthetic data discuss the impact of different levels of noise in radar data on the Active/Passive algorithm.

4.2. Test of Algorithm using Synthetic Data

The Active/Passive algorithm was applied on all the 36-km pixels of the Red-Arkansas river domain of the OSSE data (as described in the Section 3), to evaluate the slopes $\beta_{vv}(\mathrm{C})$ and $\beta_{hh}(\mathrm{C})$ from the co-polarized (VV and HH) backscatter $\sigma_{vv}(F_m,t)$ and $\sigma_{hh}(F_m,t)$, respectively. A higher correlation for VV than HH was found between the aggregated $\sigma(\mathrm{F_m},\mathrm{t})$ and $\theta(C,t)$ in the observing system simulation fields. Hence,

outputs based on $\sigma_{vv}(\mathrm{F_m},\mathrm{t})$ input to the algorithm yield slightly lower RMSE errors than for $\sigma_{hh}(F_m,t)$, in agreement with the results of [8]. Figure 5 illustrates a sample of the ground truth soil moisture at 9 km, the radiometer-only coarse resolution soil moisture at 36 km, the co-polarized radar backscatter $\sigma_{vv}(\mathrm{F_m},\mathrm{t})$ at 3 km, the algorithm-retrieved high resolution soil moisture $\theta_{vv}(M,t)$ at 9 km based on $\beta_{vv}(\mathrm{C})$, and VWC at 36 km for DOY 130, 1994. The retrieval result (Fig. 5d) shows that the algorithm captures the higher-resolution soil moisture variability otherwise masked by the radiometer-only coarse resolution soil moisture estimates (Fig. 5b), and exhibits the correct spatial patterns seen in the 'truth' soil moisture (Fig. 5a).

For the 122-day duration of the OSSE simulation the RMSE of the retrieved soil moisture outputs at 9-km resolution were computed to evaluate the algorithm performance. Figure 6 shows the temporal evolution of the standard deviation (Std. Dev.) and mean of the retrieved soil moisture field, and the retrieval RMSE, averaged for each day over the entire river basin (OSSE domain). The algorithm captures the typical soil moisture dynamics (Fig. 6), in which the standard deviation increases with initial drydown due to increasing spatial variability, and then gradually decreases because of dry soil surface conditions. At a regional scale, the algorithm also displays the robustness by constraining the regional RMSE fluctuations within a range of ~2.8 – 3.3% Vol. soil moisture for a corresponding range of ~7 – 12% and ~16 – 32% Vol. soil moisture in regional standard deviation and mean, respectively. It is also interesting to see that the regional RMSE stays close to 3% Vol. soil moisture for the whole duration of the study period.

The next logical step was to evaluate the improvement of the high-resolution soil moisture fields at 9 km derived from the active/passive algorithm (L2_SM_A/P) over the 'minimum performance' fields that could be derived using radiometer-only measurements. Minimum performance soil moisture field were obtained by re-sampling the radiometer-only soil moisture values at 36 km (L2_SM_P) to high resolution 9 km pixels. The soil moisture values at 36 km (L2_SM_P) represent an average estimate, and to evaluate the minimum performance against the algorithm results, the soil moisture values at 36 km are assigned to all 9 km pixels that fall within 36 km pixel. So, all the 16 pixels of 9 km resolution that are within 36 km pixel have the same soil moisture values. Hence, the minimum performance estimates at 9 km do not capture the underlying heterogeneity (variability) that is identified by the algorithm using the high resolution radar backscatter. A pixel-wise soil moisture RMSE was computed over the river basin for minimum performance (Fig. 7a) and algorithm retrieval (Fig. 7b) for the whole duration of the OSSE. Visual comparison of Fig. 7a and Fig. 7b shows an obvious improvement in soil moisture estimates when the active/passive retrieval algorithm is used. To quantify the improvement, a ratio of algorithm-based soil moisture RMSE to minimum performance RMSE is shown in Fig. 7c. The algorithm estimates outperform the radiometer only estimates (ratio less than one) over most of the river basin. In some parts of the basin the RMSE ratio is close to unity. These are the eastern and western forested regions where the radar sensitivity to soil moisture is low due to the high VWC (Fig. 5e). Apart from these regions the active/passive algorithm estimates are considerably superior to the radiometer-only estimates.

An additional analysis was conducted to examine the impact of vegetation. The spatial patterns in the retrieval errors are correlated with the distribution of vegetation within the river basin. Figure 8 plots retrieved soil moisture RMSE and minimum performance soil moisture RMSE stratified by the mean VWC contained within 9 km for the duration of OSSE. The algorithm-retrieved soil moisture RMSE shows an improvement of 0.01-0.02 cm^3/cm^3 soil moisture relative to the minimum performance RMSE over the entire VWC range. The general increase in RMSE with increase in VWC as observed in Fig. 8 is due to the masking effect of vegetation on the radar sensitivity to soil moisture and a positive bias in the retrieval. The algorithm performs well (RMSE< 0.04 cm^3/cm^3) for values of VWC below 4 kg/m^2. A sharp rise in the RMSE is observed for VWC values greater than 4 kg/m^2. A partial reason for this is that the algorithm performance as tested in this OSSE is susceptible to the low number of 9-km pixels having VWC > 2.5 kg/m^2 in the OSSE domain.

The detection of soil moisture variability within a radiometer pixel at 36 km depends on the accurate representation of this spatial heterogeneity in the high-resolution radar backscatter measurement. The inherent radar K_p measurement error confounds the actual spatial heterogeneity thereby introducing a source of error that requires quantification in retrieved soil moisture at 9 km. A sensitivity analysis of the input K_p error was performed and the RMSE results stratified by VWC are shown in Fig. 9. An increase in RMSE with increase of K_p is clearly visible in the plot. However, the impact of increasing K_p on the algorithm is not large. This is due to the averaging of $\sigma(\mathrm{F_m},\mathrm{t})$ to $\sigma(\mathrm{M_n},\mathrm{t})$ that reduces the effective K_p. This analysis reveals that the prominent error in the output from the algorithm is the error in $\theta(C,t)$.

In order to quantify the error due to the assumption on the spatial scale of variability in the slope parameter β, an experiment was carried out where β was estimated at scale M_n or 9 km (which is possible with the OSSE dataset). The parameters $\beta(M_n)$ were then used for the algorithm instead of $\beta(C)$ in (7). The thick dashed lines in Fig. 9 show that the assumption on the scale of variation of β does increase the RMSE. The increase in the soil moisture RMSE averages about 0.005 cm^3/cm^3 over the OSSE basin.

5. Discussion and Conclusion

An algorithm has been proposed in this paper for obtaining high resolution (9 km) soil moisture from SMAP coarse scale (36 km) radiometer-based soil moisture estimates and fine scale (3 km) radar-based co-polarized backscatter cross-sections. The approach takes advantage of the near-linear relationship between volumetric soil moisture and radar backscatter cross-section, and the capability of the high resolution radar backscatter to capture the spatial heterogeneity of soil moisture within the radiometer footprint. The algorithm uses time-series information to determine and refine the slope of the linear relationship and, unlike in [8] and [9], the algorithm does not require the previous satellite overpass observations to estimate the current soil moisture value. This provides greater operational flexibility. The accumulation of errors over time that is a potential feature of [8] is also not encountered in this algorithm. The algorithm output is an absolute soil moisture estimate at high resolution that is an improvement over the estimation of soil moisture relative change only as proposed by [9]. It is shown that the algorithm soil moisture retrieval accuracy relies to a large extent on the accuracy of the radiometer-based coarse resolution (36 km) soil moisture inputs, and that the effects of

radar backscatter measurement random errors can be significantly reduced by averaging to the 9-km scale. The algorithm simulations using the SMEX02 PALS data and synthetic four-month OSSE dataset are encouraging and suggest an improvement of nearly 0.015 to 0.02 cm^3/cm^3 in soil moisture retrieval accuracy over the minimum performance radiometer estimates. The L2_SM_A/P product is expected to meet the mission criterion of 0.04 cm^3/cm^3 soil moisture accuracy (one-sigma) or better for regions with VWC less than 5 kg/m^2. A few caveats in the studies performed here should be mentioned: (1) For the OSSE dataset, the confidence in the results for pixels with VWC > 2.5 kg/m^2 is limited by the low number of these pixels in the OSSE domain. (2) The RMSE of the L2_SM_A/P retrievals at 9 km can never be less than the RMSE of the overlapping L2_SM_P radiometer-only soil moisture estimates at 36 km because as an input L2_SM_P, the inherent errors in it percolate through the L2_SM_A/P algorithm. (3) Further studies are required to test the efficacy of the algorithm using real observational data (for example using airborne data sets such as acquired by PALS) obtained from different hydroclimatic regions.

The proposed Active/Passive algorithm can also be applied using radar observations at finer scales (e.g., 3 km). In this case soil moisture at finer scales (e.g. 3 km) could be estimated. However, the errors will be considerably higher because: (1) without averaging to the intermediate 9 km scale radar speckle noise will be more evident, and (2) patchiness in vegetation and azimuthal differences will increase significantly. Preliminary studies using 3 km radar backscatter cross-section from the OSSE dataset have been conducted. Results (not shown) indicate that the soil moisture retrievals generally did not meet the SMAP soil moisture accuracy requirement of 0.04

cm^3/cm^3. Only at rather low VWC levels (< 2 kg/m^2) did the 3 km soil moisture fall below 0.04 cm^3/cm^3, but it did not improve on the minimum performance benchmark. Therefore our conclusion, based on the current SMAP instrument design, is that averaging to an intermediate scale (9 km) between the radar and radiometer resolutions is needed for the application of the Active/Passive algorithm.

The algorithm needs to be tested in larger study domains that include greater diversity in surface characteristics and hydroclimatic regions, and to establish optimum time windows for determining the algorithm parameters that depend on changing surface conditions. To achieve this, future work on this algorithm will include study area for different PALS domains and global extent of OSSE that will facilitate to analyze the performance of the algorithm for wide range of ground conditions. Future studies will also aim at improved parameterization of the sensitivity/slope (β) relationship as a function of vegetation characteristics, allowing the effect of vegetation heterogeneity within the coarse radiometer footprint to be better addressed.

Acknowledgment

The authors especially thank Dr. Andreas Colliander for providing the processed PALS data for this work. The authors also wish to thank the Algorithm Development Team of the SMAP project for their guidance and assistance at various stages of this work.

References

[1] J. D. Albertson and M. B. Parlange, "Natural integration of scalar fluxes from complex terrain," *Adv. Water Resources*, vol. 23, no. 3, pp. 239–252, 2000.

[2] C. P. Weaver, and R. Avissar, "Atmospheric disturbances caused by human modification of the landscape," *Bull. Am. Meterol.* Soc., vol. 82, pp. 269-281, 2001.

[3] "Earth Science and Applications from Space: National Imperatives for the next Decade and Beyond," National Research Council, http://www.nap.edu, 2007.

[4] D. Entekhabi, E. G. Njoku, P. E. O'Neill, K. H. Kellogg, W. T. Crow, W. N. Edelstein, J. K. Entin, S. D. Goodman, T. J. Jackson, J. Johnson, J. Kimball, J. R. Piepmeier, R. D. Koster, N. Martin, K. C. McDonald, M. Moghaddam, S. Moran, R. Reichle, J. C. Shi, M. W. Spencer, S. W. Thurman, L. Tsang, and J. V. Zyl, "The Soil Moisture Active Passive (SMAP) Mission," Proceedings of the IEEE, vol. 98, pp. 704-716, 2010.

[5] E. G. Njoku, and D. Entekhabi, "Passive microwave remote sensing of soil moisture," *J. Hydrol.*, vol. 184, pp. 101-129, 1996.

[6] F. T. Ulaby, P. Dubois, and J. V. Zyl, “Radar mapping of surface soil moisture," *J. Hydrol.*, vol. 184, pp. 57-84, 1996.

[7] Y. Kim, and J. van Zyl, “A Time Series Approach to Estimate Soil Moisture Using Polarimetric Radar Data,” *IEEE Trans. Geosci. Remote Sens*. vol. 47, pp. 2519-2527, 2009..

[8] M. Piles, D. Entekhabi, and A. Camps, “A Change Detection Algorithm for Retrieving High Resolution Soil Moisture from SMAP Radar and Radiometer Observations,” *IEEE Trans. Geosci. Remote Sens*., vol. 47, pp. 4125-4131, 2009.

[9] U. Narayan, V. Lakshmi, and T. J. Jackson, “High resoluiton estimation of soil moisture using L-band radiometer and radar observations made during the SMEX02 experiments,” *IEEE Trans. Geosci. Remote Sens.*, vol. 44, pp. 1545-1554, 2006.

[10] Y. Du., F. T. Ulbay, and M. C. Dobson, “Sensitivity to soil moisture by active and passive microwave sensors,” *IEEE Trans. Geosci. Remote Sens.*,vol. 38, pp. 105-114, 2000.

[11] W. J. Wilson, S. H. Yueh, S. J. Dinardo, S. Chazanoff, F.K. Li, and Y. Rahmat-Samii, “Passive Active L- and S-band (PALS) microwave sensor for ocean salinity and soil moisture measurements,” *IEEE Trans. Geosci. Remote Sens*., vol. 39, pp. 1039-1048, 2001.

[12] W. T. Crow, S. T. D. Chan, D. Entekhabi, P. R. Houser, A. Y. Hsu, T. J. Jackson, E. G. Njoku, P. E. O’Neill, J. Shi, and X. Zhan, “An Observing System Simulation Experiment for Hydros Radiometer-Only Soil Moisture Products,” *IEEE Trans. Geosci. Remote Sens.*, vol. 43, pp. 1289-1303, 2005.

[13] X. Zhan, P. R. Houser, J. P. Walker, and W. T. Crow, “A Method for Retrieving High-Resolution Surface Soil Moisture From Hydros L-Band Radiometer and Radar Observations,” *IEEE Trans. Geosci. Remote Sens.*, vol. 44, pp. 1534-1544, 2006.

Table 1. Proposed data products from the SMAP mission.

Data Product Short Name	Description	Data Resolution
L1B_S0_LoRes	Low Resolution Radar σ_o in Time Order	5x30 km
L1C_S0_ HiRes	High Resolution Radar σ_o on Swath Grid	1-3 km
L1B_TB	Radiometer T_B in Time Order	36x47 km
L1C_TB	Radiometer T_B on Earth Grid	36 km
L2_SM_P	Radiometer Soil Moisture	36 km
L2_SM_A	Radar Soil Moisture	3 km
L2_SM_A/P	Active/Passive Soil Moisture	9 km
L3_F/T_A	Daily Global Composite Freeze/Thaw State	1-3 km
L3_SM_P	Daily Global Composite Radiometer Soil Moisture	36 km
L3_SM_A/P	Daily Global Composite Active/Passive Soil Moisture	9 km
L4_SM	Surface & Root Zone Soil Moisture	9 km
L4_C	Carbon Net Ecosystem Exchange	1 km

Figures

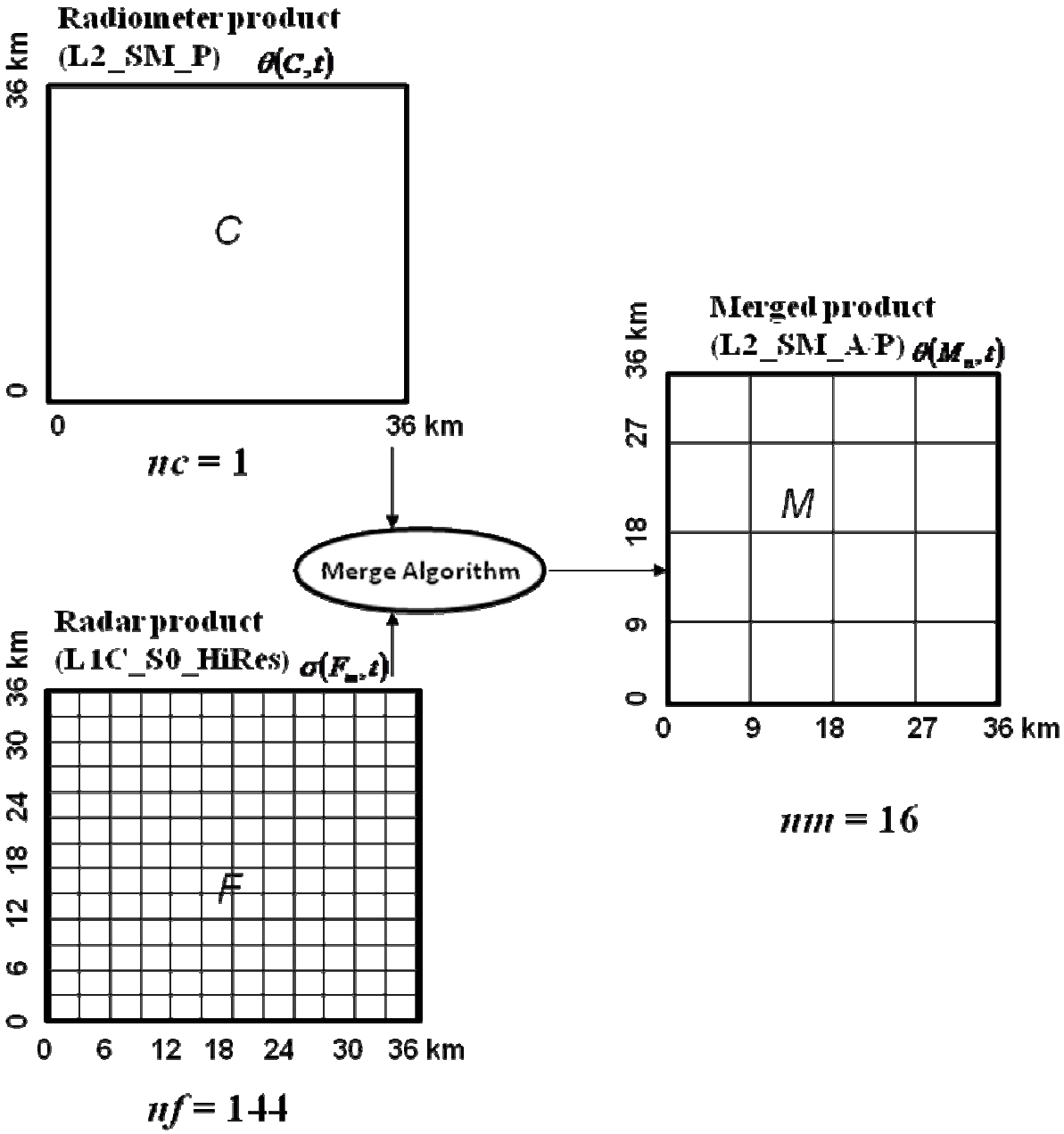

Figure 1: Grid topology of radiometer (L2_SM_P), radar (L2_SM_A), and merge (L2_SM_A/P) product. Where *nf* and *nm* are number of area pixels of radar and merged product, respectively, within one radiometer area pixel *nc*.

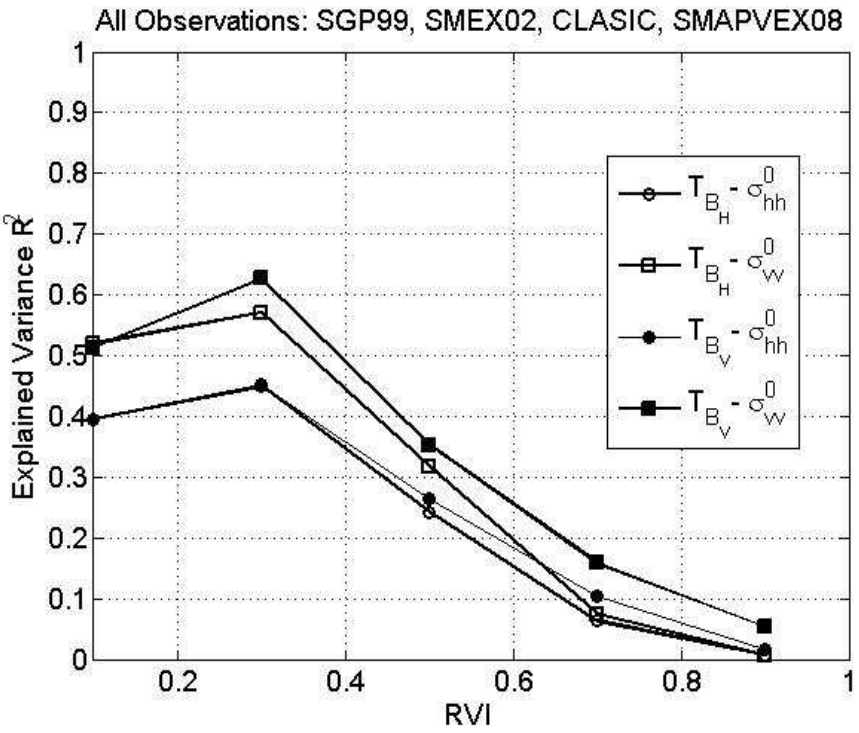

Figure 2: Correlations between different combinations of T_{B_p} and σ_{pp} with respect to radar-vegetation-index (RVI) evaluated from PALS data taken over four field experiments.

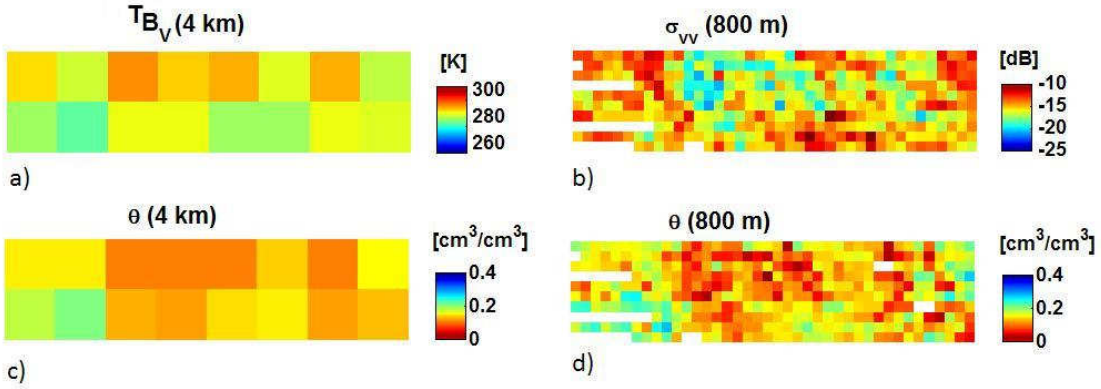

Figure 3: a) Averaged and gridded T_{B_V} SMEX02 PALS data (4 km) for 5th July, 2002, b) Averaged and gridded σ_{vv} SMEX02 PALS data (0.8 km) for 5th July, 2002, c) Retrieved soil moisture estimates from T_{B_V} SMEX02 PALS data (4 km) for 5th July, 2002, and d) Disaggregated soil moisture estimates from Active/Passive algorithm for 5th July, 2002.

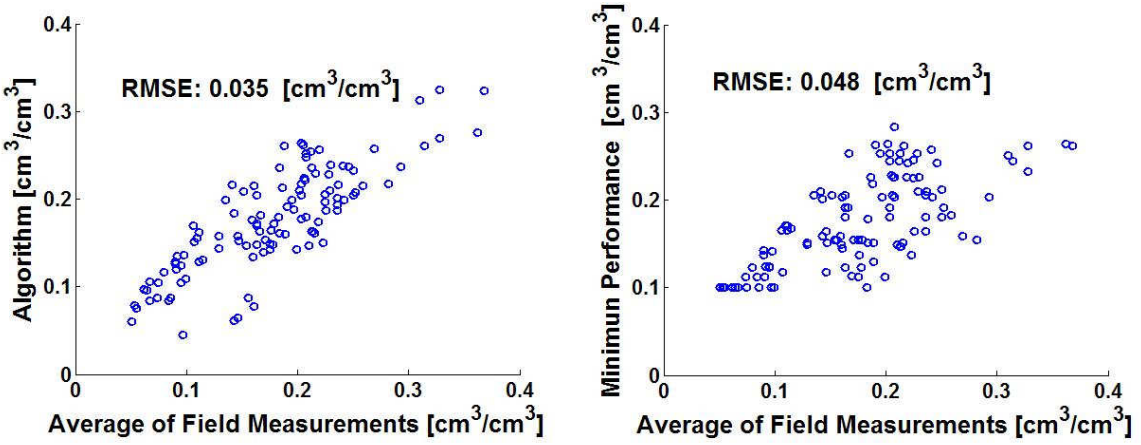

Figure 4: Plots of averaged soil moisture from field measurements and retrieved soil moisture estimate from PALS data for 4 days. a) Active/Passive algorithm, and b) Minimum performance.

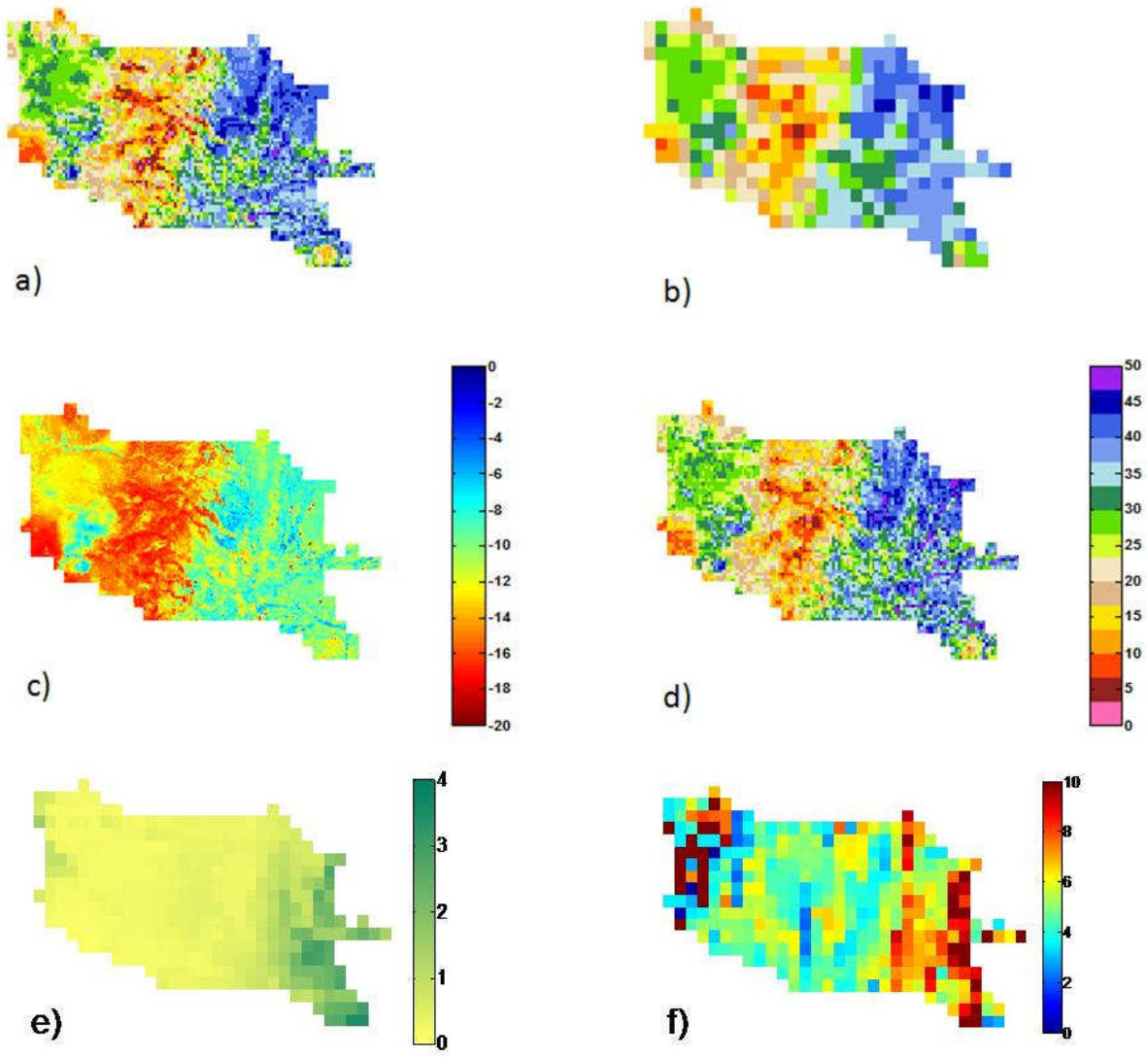

Figure 5: Surface soil moisture fields of Red-Arkansas river basin on DOY 130, 1994. a) Synthetic ground truth soil moisture (9 km), b) Radiometer derived soil moisture (36 km), c) Radar backscatter $\sigma_{vv}(M_n,t)$ with Kp = 0.16, d) Soil moisture field (9 km) obtained from the algorithm, e) VWC (kg/m^2)at 36 km resolution, and f) Derived slope (β) between radiometer-based Soil moisture estimate (L2_SM_P) at 36 km and $\sigma_{vv}(M_n,t)$ aggregated to 36 km spatial resolution.

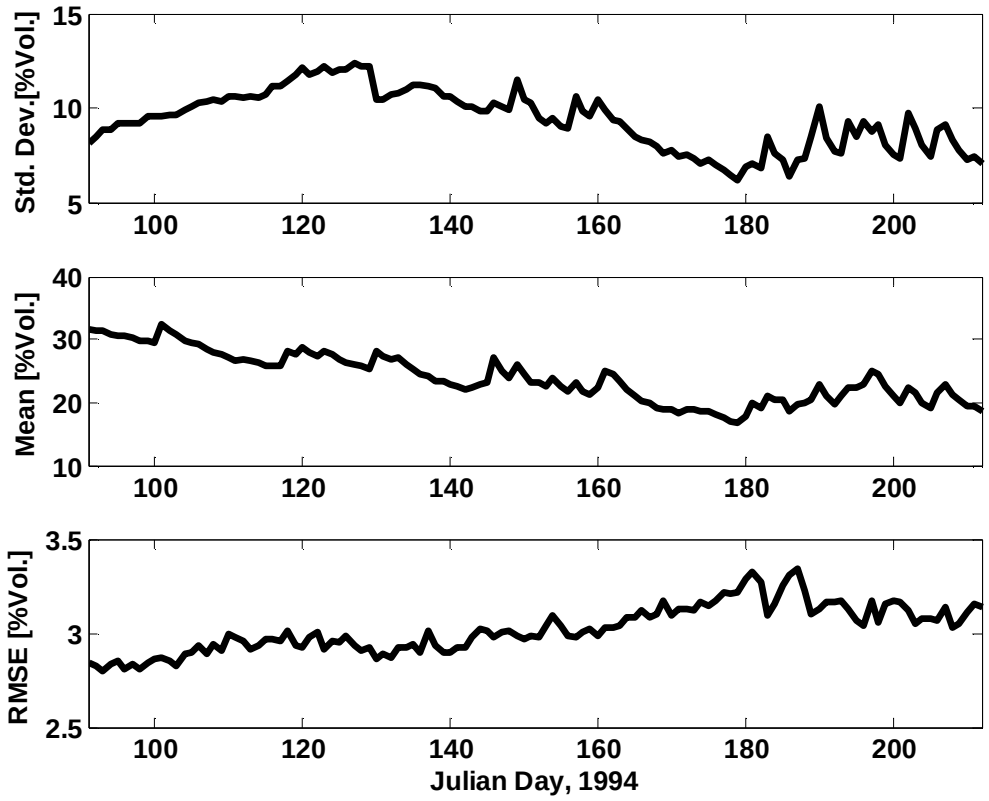

Figure 6: Region standard deviation, mean and RMSE computed from algorithm derived soil moisture estimates at 9 km for the whole duration of OSSE. The line in 3c represents the RMSE using β estimated at 36 km. (Results based on four-months synthetic OSSE dataset).

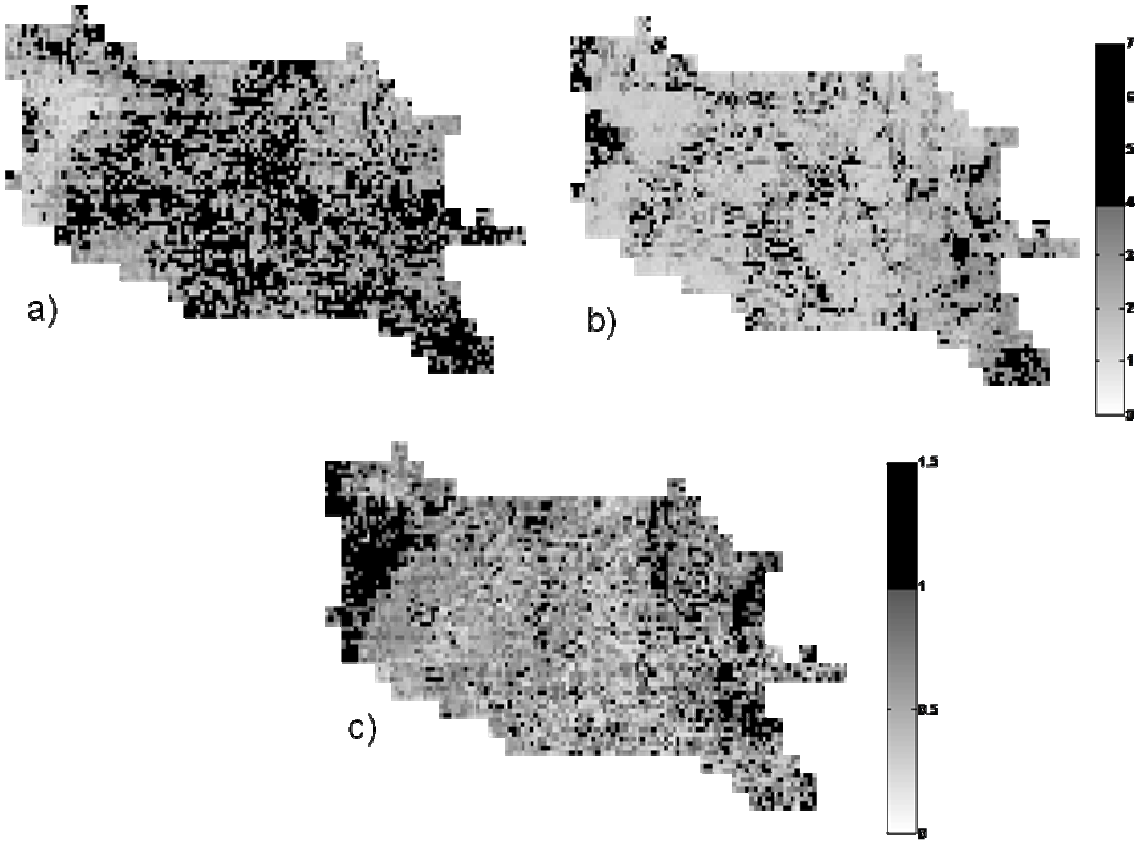

Figure 7: a) Pixel-wise average RMSE of minimum performance radiometer only soil moisture, b) Pixel-wise average RMSE of algorithm derived soil moisture estimates using $\sigma_{vv}(M_n,t)$ having Kp = 0.16 and $\theta(C,t)$ having RMSE of 1 to 4 %Vol. soil moisture for pixels having VWC from 0 to 5 kg/m2, respectively, and c) Ratio of algorithm-based pixel-wise average RMSE to radiometer only minimum performance pixel-wise average RMSE. (Results based on four-months synthetic OSSE dataset).

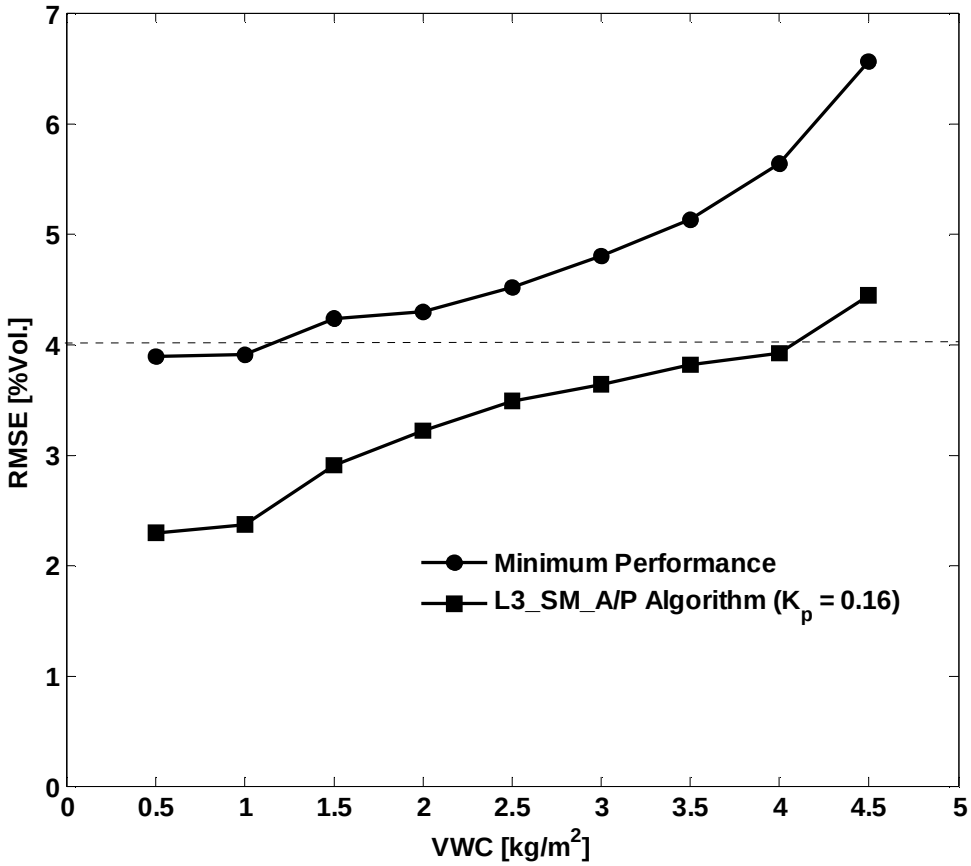

Figure 8: Average RMSE for minimum performance and algorithm derived soil moisture estimates stratified by VWC. (Results based on four-months synthetic OSSE dataset).

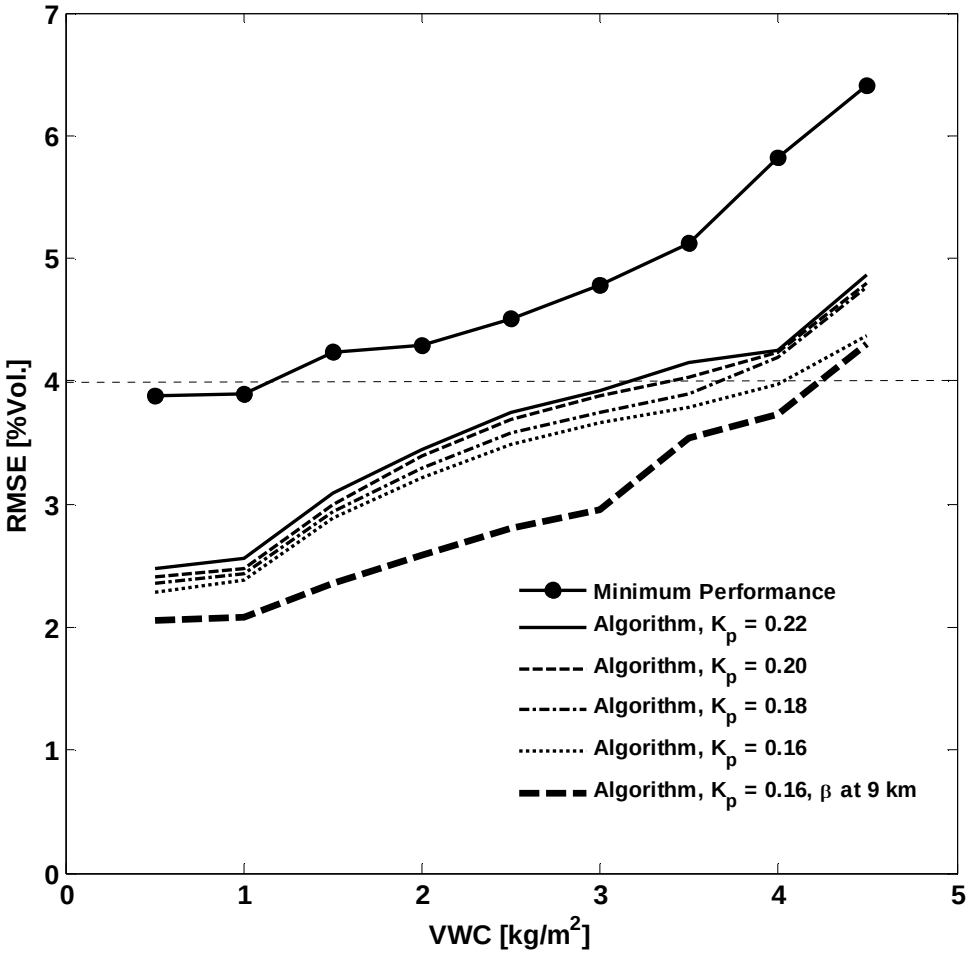

Figure 9: Sensitivity analysis of the input errors in L1C_S0_HiRes subjected to the algorithm. The thick dashed line shows the RMSE with β estimated at 9 km. (Results based on four-months synthetic OSSE dataset).